Regular Article

PHYSICAL CHEMISTRY RESEARCH
Published by the
Iranian Chemical Society
www.physchemres.org
info@physchemres.org

Phys. Chem. Res., Vol. 11, No. 4, 771-782, December 2023
DOI: 10.22036/pcr.2022.351688.2137

Synthesis of TiO_2 Nanoparticles by Hydrothermal Method and Characterization of their Antibacterial Activity: Investigation of the Impact of Magnetism on the Photocatalytic Properties of the Nanoparticles

H.G. Hameed* and N.A. Abdulrahman

Department of Chemistry, College of Science, University of Baghdad, Baghdad, Iraq

(Received 13 July 2022, Accepted 6 November 2022)

TiO_2-NPs were proven to be effective antibacterial agents. In this work, hydrothermal processing was used to synthesize TiO_2-NPs, and their photocatalytic, and antibacterial activities were investigated. In addition, this research has explored the effects of magnetic field in the hydrothermal synthesis of TiO_2-NPs. FE-SEM, UV-VIS, EDX, and XRD were used to analyze the TiO_2-NPs. The use of a magnetic field in the hydrothermal synthesis of TiO_2-NPs (Treated) has led to the successful formation of TiO_2 nano rode in shape compared with untreated particles (No magnetic field) which exhibit no definite shape. Antibacterial activities were performed against two of the most important bacteria strains that cause disease in humans: *Staphylococcus aureus* (*S. aureus*) and *Escherichia coli* (*E. coli*). The treated TiO_2-NPs exhibited enhanced antibacterial activity when compared with untreated TiO_2-NPs samples. The treated TiO_2-NPs show a greater efficacy on antibacterial properties compared to the untreated TiO_2 NPs. In addition, the photocatalytic activity of TiO_2-NPs has been investigated by applying the photodegradation of the methylene blue (MB) method using UV light under neutral conditions. The findings have proved that the degradation efficiency of MB dye in an aqueous solution has been affected by the irradiation time. Also, treated TiO_2-NPs had a high photodegradation efficiency of 96% of the dye after 3 hours compared with untreated samples recorded at only 21%.

Keywords: Hydrothermal method, TiO_2 nanoparticles, FE-SEM, Antibacterial, XRD

INTRODUCTION

The environment around people has gotten worse as a result of different contagious illnesses, which are mostly carried by bacteria. Microbes harm the environment, the health sector, the food sector, and the textile sector. The greatest method to reverse this harm was to develop the best and most effective antibacterial agent available. The antibacterial properties of nanoparticles, in particular metal oxide nanoparticles, assist to eliminate the harm caused by germs [1]. These substances were divided into two categories, namely organic and inorganic substances [2]. In comparison to the other two classes, inorganic materials have shown exceptional resistance to microorganisms [3]. Even at low concentrations, metal oxide nanoparticles have strong antibacterial action. Numerous inorganic oxides showed strong antibacterial action, including TiO_2, Al_2O_3, ZnO, CuO, CuO, MgO, Ag_2O, and CaO [4,5]. With a high band gap of 3.2 eV, titanium dioxide (TiO_2) is a superior photocatalyst that is employed in semiconductor applications [6,7] and dye-sensitized solar cells [8]. Due to their generation of ROS when exposed to UV radiation, they have a significant impact on stopping the development of bacteria [9]. They work well as an antibacterial agent. Because of its superior biocompatibility and photocatalytic capabilities, TiO_2 has become more widely employed. The formation of reactive oxygen and nitrogen species during the oxidation and reduction of H_2O was discovered to be the key step in many photocatalytic reactions. When it comes to TiO_2

*Corresponding author. E-mail: ismaaalmuswie@gmail.com

nanoparticles, this is unquestionably true. The ability of TiO_2 nanoparticles to produce Reactive Oxygen Species (ROS) has been linked to their antibacterial and photocatalytic characteristics [10,11]. The accumulation of bioproducts on TiO_2 surfaces can significantly increase ROS production, leading to enhanced photocatalytic and biological activity [12]. They also work well as anticancer agents because cancer cells have propensity to produce an excessive amount of reactive oxygen species when exposed to them [13].

Most substances react to magnetic fields by forming their own magnetic fields. Every substance has its unique magnetism, which is one of its primary physical characteristics. There are three different types of magnetism: diamagnetism, paramagnetism and ferromagnetism. Examples of compounds with ferromagnetic characteristics include iron and nickel. Materials that are drawn to magnetic fields are known as paramagnetic materials; an example of this is oxygen gas. Materials that are unaffected by magnetic fields are known as diamagnetic materials. This category includes water. These magnetic characteristics result from the material's magnetic susceptibility or magnetic energy density. It follows that the physical characteristics, which may be utilized to regulate physical and chemical processes, would be affected by the magnetic field [14]. Four different categories of effects caused by magnetic fields have been established: the magneto-thermodynamic effect, the quantum effect, the magnetic force, and the magnetic torque and alignment [15,16]. Since high magnetic fields are important, considerable research on the effects of magnetic fields in regulating chemical and physical processes was conducted in Japan between 1992 and 1994. According to a study titled "Innovative Utilization of High Magnetic Field," several intriguing occurrences that are difficult to notice in low magnetic fields have been seen [17]. It is important to note that even diamagnetic materials can be affected by these chemical and physical processes.

TiO_2 nanoparticles were synthesized using a variety of techniques, including chemical [18], radiation [19], electrochemical [20], and photochemical processes [21]. Hydrothermal synthesis of nanoparticles has received considerable attention in recent years because nontoxic chemicals, anticancer, antibacterial, antiviral, diagnostic, targeted drug delivery, environmentally friendly solvents, and renewable materials are becoming increasingly necessary [22-24]. The maintenance of microbial cultures is a labor-intensive procedure; thus, the hydrothermal synthesis of nanoparticles is more favorable since it can be appropriately expanded for large-scale nanoparticle synthesis. If the nanoparticles could be produced more quickly in the reaction vessels, hydrothermal synthesis would be more commercially viable. One of the most frequent methods for the synthesis of nanoparticles under high temperature and pressure is hydrothermal [25]. The advantages of the hydrothermal synthesis approach include high-crystallized powders with narrow particle size distribution, high purity, and process conditions such as solute concentration, as well as the ease of large-scale manufacturing [26].

In the current work, treated and untreated TiO_2-NPs were synthesized using hydrothermal method. The nanoparticles were characterized using XRD, FE-SEM, EDX, and UV-Vis spectroscopy. The antibacterial nature of the treated and untreated TiO_2-NPs was evaluated against gram-positive and gram-negative bacteria using well diffusion method. In addition, the photocatalytic activity of synthesizes TiO_2-NPs has been evaluated.

MATERIALS AND METHODS

Materials

All the materials used in the current research were acquired from Sigma -Aldrich Chemicals which are: Titanium tetra isopropoxide (TTIP) with M.Wt = 284.2 g mol^{-1}, purity = 97%) and potassium hydroxide (KOH). A Handheld Gauss Meter tesla meter was used to measure the applied magnetics strength.

Hydrothermal Synthesis of TiO_2-NPs under Magnetic Field

By using a hydrothermal process, titanium dioxide nanoparticles under magnetic fields (treated TiO_2-NPs*)* have been synthesized. 50 ml of a 0.1 M TTIP solution was placed inside a cold-water bath till the temperature range of (3-5 °C) was obtained. After that, 5.0 M KOH was gradually added to the cold solution until pH 7.0 was achieved. Then, the obtained mixture was transferred to a Teflon autoclave and then subjected to a temperature of about 160 °C for 5 h. Then, the solution mixture was then placed under a magnetic field

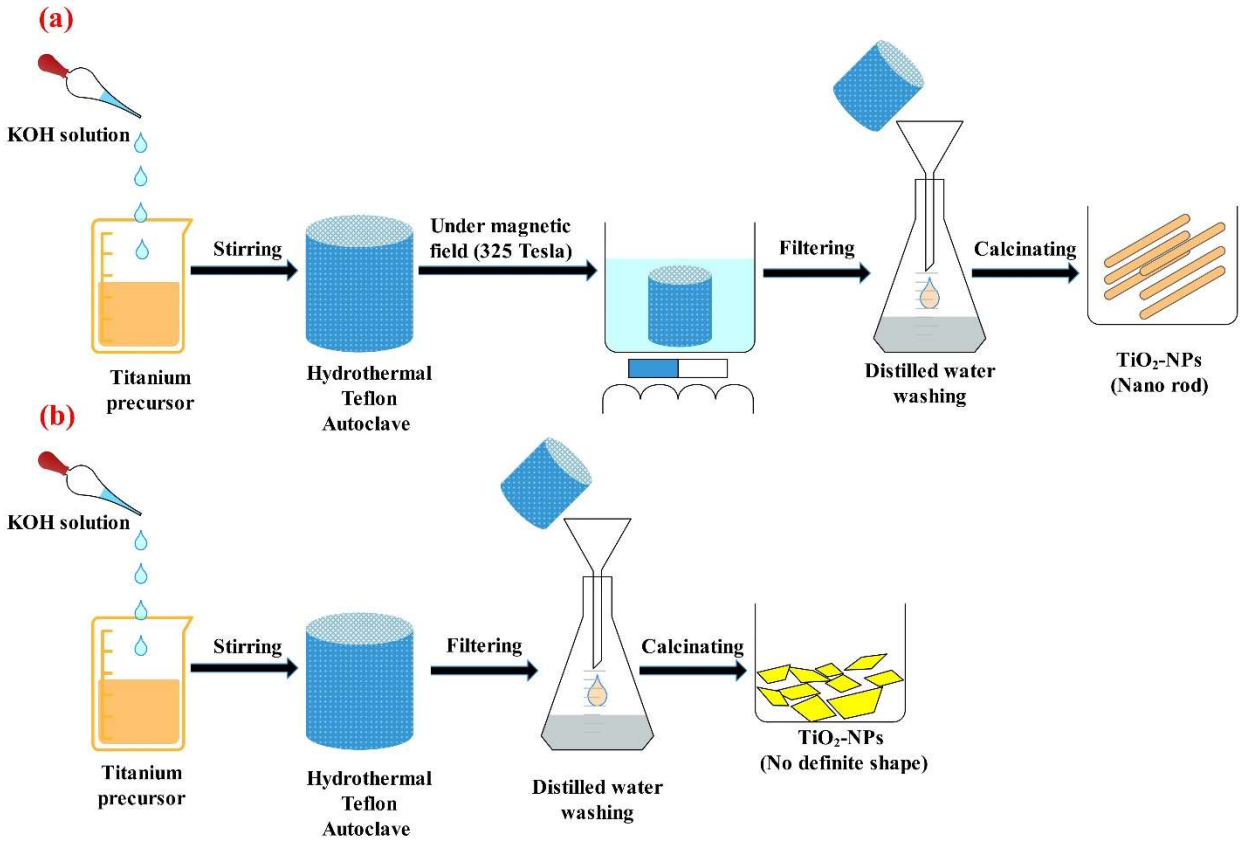

Fig. 1. Schematic showing various steps of the hydrothermal method involved in (a) alkaline-hydrothermal under magnetic field and (b) alkaline-hydrothermal without magnetic field.

(3.25 Tesla). Then, the solution was centrifuged at speed of 5000 rpm for 10 to 15 min and then rinsed with distilled water to get rid of impurities and then kept in an oven at 100 °C for 20 h. The obtained TiO_2 powder was annealed for 2 h at 450 °C for further preparation. While the untreated TiO_2-NPs, it was synthesized by following the same above procedure except for the magnetic step. The whole procedure is shown in Fig. 1.

Characterization Techniques

Using a UV-Vis spectrophotometer, the powders of treated TiO_2-NPs and untreated TiO_2-NPs were examined spectrally in the 200-800 nm region. X-ray diffraction (XRD) examination was used to determine the sample's crystallinity utilizing the XPERT-PRO, which was run at 45 kV, 40 mA, and a 2θ angle pattern. With a 300 kV accelerating voltage, the FE-SEM-JEOL-3010 was used to conduct the FE-SEM tests. The Energy-dispersive X-ray spectroscopy (Type S-4800 Hitachi, Japan) was used for complete microanalysis of TiO_2-NPs.

The Photocatalyst Assay of TiO_2-NPs

In order to study the photocatalytic activities of synthesized TiO_2-NPs (Untreated and treated), the methylene blue (MB) degradation method was applied using UV light. Therefore, to allow the adsorption-desorption equilibrium to be felt, the test tube containing the TiO_2-NPs and 10 ml of a 10 µg m^{-1} MB solution was covered with aluminum foil and shaken for 15 min at 25 °C in the dark. Following that, a 100 W xenon lamp was used to illuminate the reaction mixture in a time-dependent manner. 2.5 ml of the solution's volume was taken out of the conical at organized during illumination. The TiO_2-NPs were separated by centrifugation at the precise irradiation time, and the absorption was then determined using a spectrophotometer. The degradation percentage of MB dye was calculated using the following

equations:

$$\text{The rate of degradation (\%)} = \frac{C_0 - C}{C_0} \times 100 \quad (1)$$

$$\text{The rate of degradation (\%)} = \frac{A_0 - A}{A_0} \times 100 \quad (2)$$

Where the C_0 is the initial concertation of MB dye in μg ml^{-1} and C is the concentration of MB dye after irradiation in μg ml^{-1}. A_o and A are the absorbances of MB dye before and after irradiation respectively.

Antibacterial Assay

By using the agar well diffusion technique, the antimicrobial activities of both treated TiO_2-NPs and untreated TiO_2-NPs were assessed [27]. *Escherichia coli* (MTCC 443) and *Staphylococcus aureus* were the test organisms utilized for the antimicrobial analysis, and they were obtained from the Microbial Type Culture Collection and Gene Bank (MTCC) in Chandigarh. Nutrient agar was used to sustain the bacterial strains.

Antimicrobial experiment. To prepare the medium, 1000 cc of distilled water was diluted in 38 g of Muller Hinton agar (Hi media). After that, it was autoclaved for one-fourth of an hour at 120 °C and 15 Lbs of pressure (pH = 7.3).

After being well mixed and allowed to cool, it was then put into the petri dish. *E. coli* and *S. aureus* pathogenic bacterial cultures were used to swab the plates before specimens were added to the wells that had been 6 mm drilled into the Muller Hinton medium. The plates were then incubated in an incubator for approximately 24 h at 37 °C. Then, the millimeters of the zone of inhibition was measured. The usual control utilized was streptomycin.

RESULTS AND DISCUSSION

UV Investigations of Treated and Untreated TiO_2-NPs

The UV spectra of the samples that were synthesized are shown in Fig. 2. For the treated and untreated TiO_2-NPs samples, the absorption profile was slightly different. In the case of untreated TiO_2-NPs, the greatest absorbance was noted at 338 nm. Similar results were achieved for pure TiO_2 nanoparticles at 337 nm and 338 nm respectively and were reported in the literature [28,29]. The chemisorption of molecules of onto the surface of treated TiO_2-NPs samples causes the absorbance maximum to be somewhat red-shifted. A maximum absorbance of 348 nm, is noted for the treated TiO_2-NPs samples. This change shows that the magnetic field has led to a significant interaction between the TiO_2 nanoparticles. Because of this, it is evident that the magnetic field changed the TiO_2's surface. The red-shifted at the TiO_2 absorption edge is a definite indication that the treated TiO_2-NPs have greater particle sizes than the untreated samples.

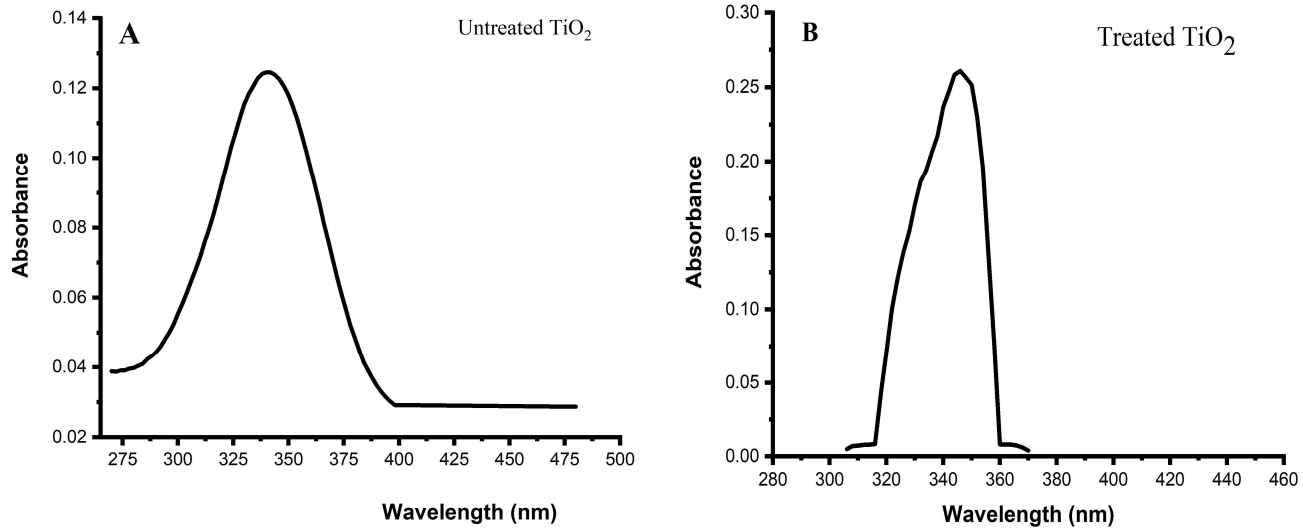

Fig. 2. The UV spectra of (A) untreated TiO_2-NPs and (B) Treated TiO_2-NPs. All the samples were synthesized under 190 °C.

Additionally, the FE-SEM study shows this increase in particle size. The narrow band gap is attributed to the increase in particle size, which in turn leads to greater electron and hole pair production.

Determination of the Energy Gap Band of Synthesized TiO_2-NPs (Treated and Untreated)

The energy required to excite an electron from the valence band to the conduction band is known as the band gap energy of a semiconductor. In order to accurately anticipate the photophysical and photochemical characteristics of semiconductors, the band gap energy must be determined. When discussing the photocatalytic characteristics of semiconductors, in particular, this parameter is frequently mentioned. Tauc put out an approach in 1966 that used optical absorption spectra to gauge the band gap energy of amorphous semiconductors. On the presumption that the energy-dependent absorption coefficient may be stated by the following equation, the Tauc technique is established. Therefore, the band gap of TiO_2-NPs has been calculated from the absorption spectrum using the following equation:

$$(\varepsilon h\upsilon) = C(h-E_g)^n$$

Where the ε is the coefficient of molar extinction, E_g is the band energy in the average of TiO_2-NPs, and the n is based on the type of transition and C is a constant. E_g is the direct allowed band gap when n = ½.

As illustrated in Fig. 3 and Table 1, the average band gap of TiO_2-NPs was calculated from the intercept of the linear relation of the $(\varepsilon h\upsilon)^2$ *vs*. hυ plots on the hυ axis. Due to quantum confinement, it has been discovered that the band gap values of treated TiO_2-NPs (3.46 eV) are larger than those of untreated TiO_2-NPs (3.26 eV).

Table 1. The Values of Energy Gap for TiO_2 Nanoparticles that Synthesized with and without Magnetic Field at 190 °C, which were Calculated Using Tauc Method

Samples	Wavelength (nm)	Energy band gap (eV)
Untreated TiO_2-NPs	338	3.26
Treated TiO_2-NPs	348	3.46

The Photodegradation Study of MB Dye

The intensity of the UV-Vis spectrum, in which the MB dye has the maximum absorption at 659 nm, was used to intentionally cause MB dye photodegradation. The treated TiO_2-NPs showed that the degradation of (MB) increased progressively with exposure time. In a similar experimental setting, the treated TiO_2-NPs destroyed more than 96% of the MB dye after 3 h, while the untreated TiO_2-NPs degraded only approximately 21% of the MB dye and after 3 h, the dye degradation remained nearly constant, as shown in Fig. 4.

In addition, the experiment under the same condition was repeated but this time, the degradation of MB dye was calculated without using the UV light. The results have shown that only 5% of MB dye was degraded. This result can be explained by the following fact the photodegradation process has not occurred and the degradation of MB dye has occurred due to the MB dye has been adsorbed on the surface of TiO_2-NPs. The photoactinic mechanism of TiO_2-NPs can be clarified as shown in Fig. 5.

Morphological and Size of Treated and Untreated TiO_2-NPs Samples

Figure 6 displayed FE-SEM images of samples of TiO_2-NPs that had been synthesized at various conditions (Under magnetic and non-magnetic fields) after being calcined at 450 ºC for an hour. Using this method, the nanoparticles synthesized under magnetic field (Treated TiO_2-NPs) were effectively agglomerated into well-uniform rod-like forms of multiple diameters, as seen by FE-SEM images. The findings demonstrate that when the preparation step is included using magnetic field, the nanorods' shape is formed with variable average lengths. The reason for these variations in the shape and average lengths of the rods is that by using the magnetic field during the synthesis step, more nuclei are produced during the reaction period. While the TiO_2-NPs synthesized under non-magnetic field (Untreated TiO_2-NPs) were agglomerated into none uniformly shape. This could be because the weak van der Waals forces in the initial bonds of the complex titanium glycolate will start to break down, resulting in a reduction in the number of formed nanoparticles and in the average lengths of the formed TiO_2-NPS nanorods. Therefore, the shape of TiO_2-NPs

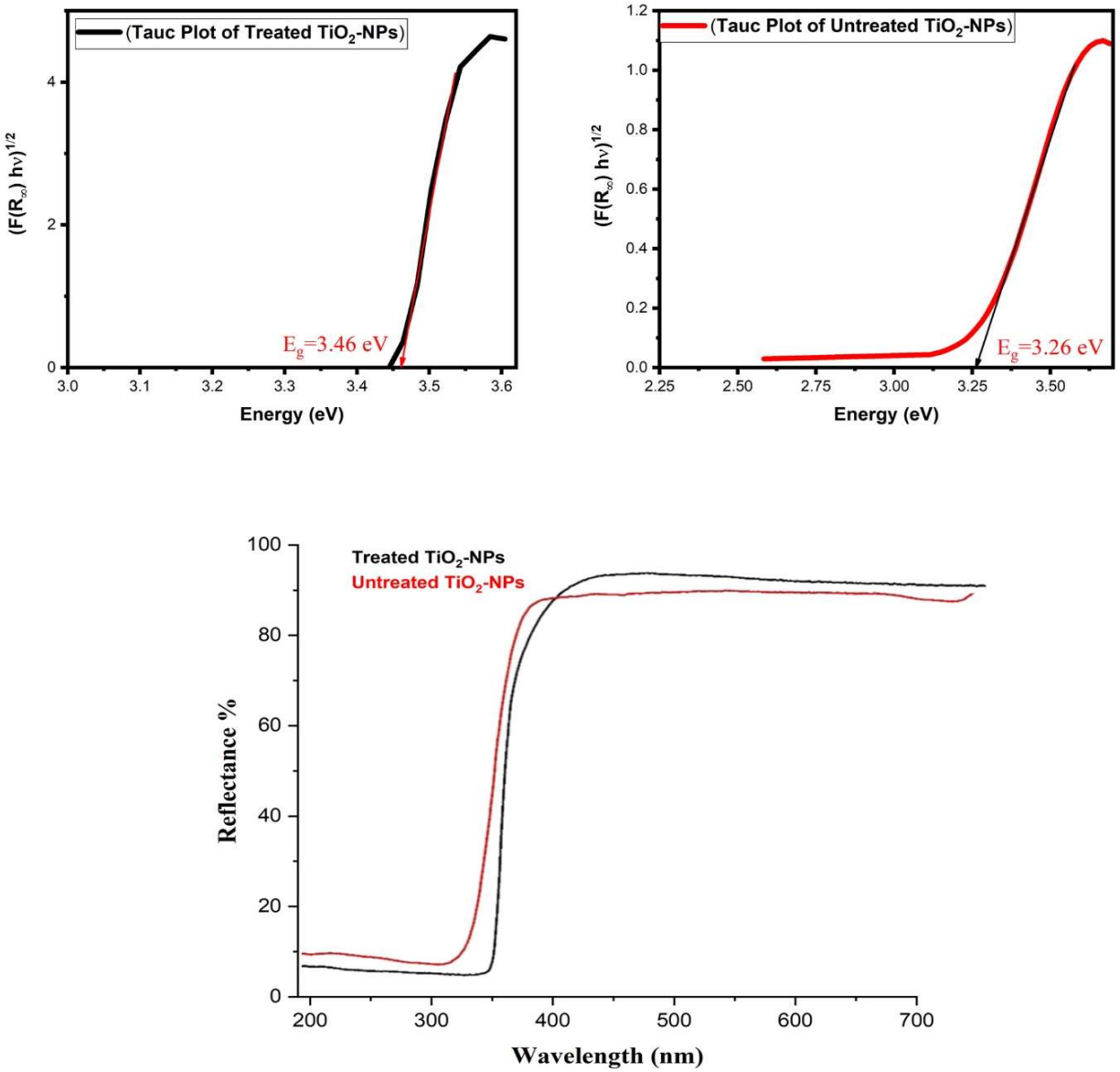

Fig. 3. The Tauc plots for the estimation of band gap for untreated TiO_2-NPs (A) and treated TiO_2-NPs (B) synthesized using the hydrothermal method at 190 °C. The diffuse reflectance spectra (DRS) of the synthesized TiO_2-NPs (Treated and untreated) samples (C).

synthesized under non-magnetic field has no definite shape. From the FE-SEM images of both types, the average size dimeters of prepared TiO_2-NPs were shown about 14.46 and 72.55 nm at synthesis temperature 190 ºC for treated and untreated TiO_2-NPs respectively.

The nitrogen adsorption and desorption isotherms illustrated in Fig. 7 were used to calculate the surface area and porosity of the synthesized TiO_2-NPs. According to the IUPAC classification, the isotherms of the obtained samples show a progressive adsorption-desorption branch with a wide range of pressure (P/P_0), which showed the presence of a mesoporous structure with a type IV pattern. Treated TiO_2-NPs samples synthesized at 190 ºC had specific surface areas of around 48.55 $m^2\ g^{-1}$, while the untreated TiO_2-NPs has 77.17 $m^2\ g^{-1}$. The plots of the pores size distribution explored using the BJH technique of the desorption branch are shown

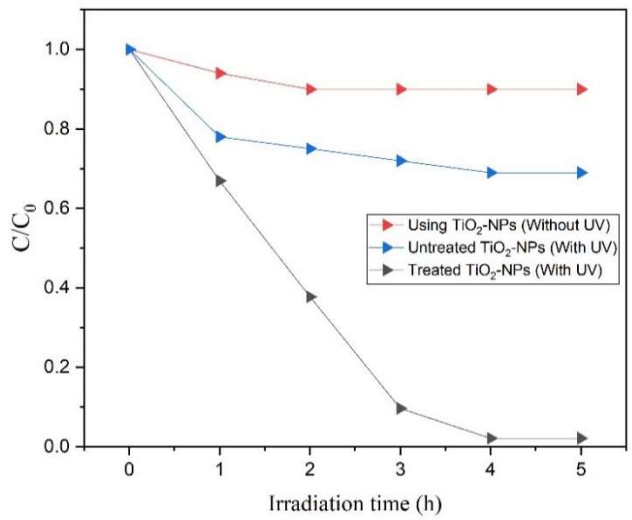

Fig. 4. Illustrates the Photocatalytic activity of TiO_2-NPs in the aqueous solution of MB dye.

$$TiO_2 + h\upsilon \longrightarrow e_{cb}^- + h_{h\upsilon}^+$$

$$h_{h\upsilon}^+ + H_2O \longrightarrow H^+ + HO^*$$

$$e_{cb}^- + O_2 \longrightarrow O_2^{-*}$$

$$O_2^{-*} + H^+ \longrightarrow HO_2^*$$

$$HO_2^* + HO_2^* \longrightarrow H_2O_2 + O_2$$

$$H_2O_2 + e_{cb}^- \longrightarrow HO^* + HO^-$$

$$H_2O_2 + h\upsilon \longrightarrow 2\,HO^*$$

$$R + HO^* \longrightarrow CO_2 + H_2O$$

Fig. 6. The mechanism of reaction between the TiO_2-NPs and MB dye during the photodegradation process.

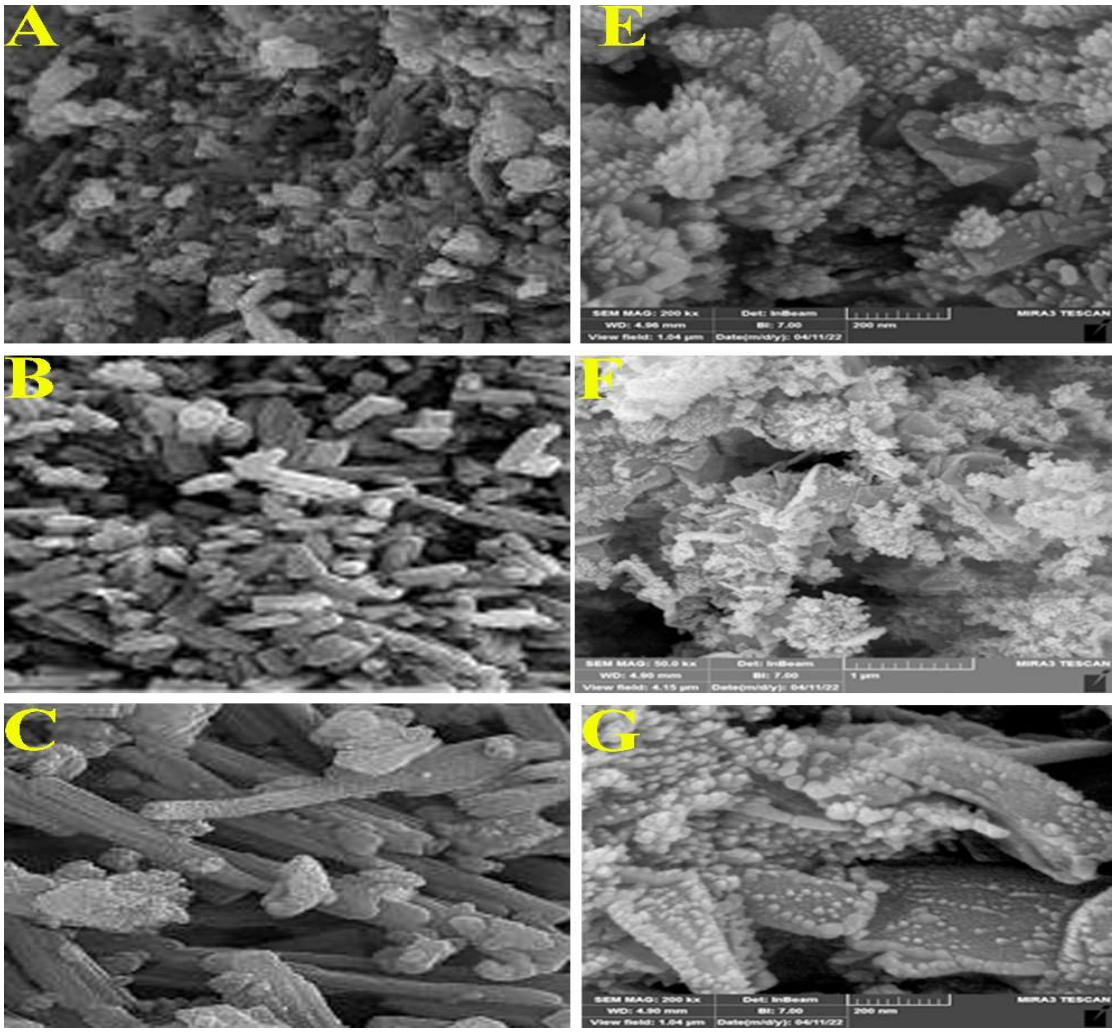

Fig. 5. FE-SEM images of treated TiO_2-NPs (A-C); untreated TiO_2-NPs (E-G) at selected temperature 190 ºC.

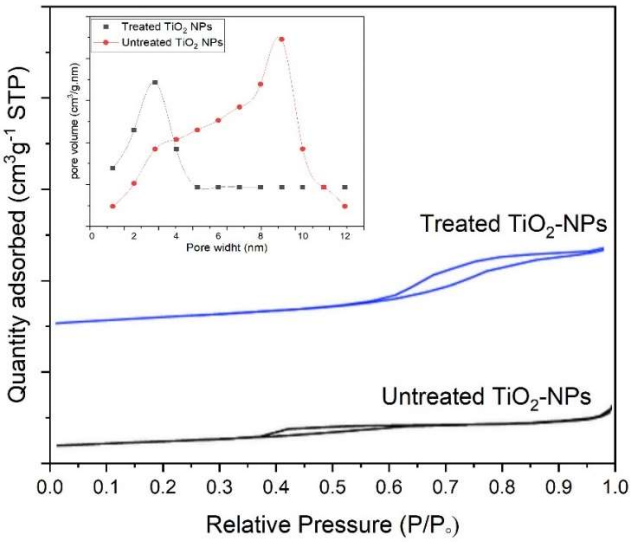

Fig. 7. The pore size distributions and the isotherm of N_2 adsorption-desorption of the synthesized TiO_2-NPs (Treated and untreated).

highlighted in Fig. 7 to assess the pores size of the generated samples. At certain temperatures, the TiO_2 mesoporous nanostructure's average pore sizes were 7.6 and 9.52 nm for treated and untreated TiO_2-NPs respectively.

Ti and O elements have been found in the TiO_2-NPs samples, as shown by corresponding EDX spectra in Fig. 8. When compared to the nominal composition of $Ti_{33.3}$. $O_{66.7}$, the chemical composition of the TiO_2-NPs samples is found to be $Ti_{37.2}O_{62.8}$, suggesting a little under stoichiometric O concentration.

Structural Investigation of Treated and Untreated TiO_2-NPs Samples

Powder XRD technique was used to characterize the nanoparticles that were synthesized using the hydrothermal method. The TiO_2-NPs' XRD pattern is seen in Figure 8. Peaks at 25.3^{θ}, 37.6^{θ}, 48^{θ}, 54.7^{θ}, 63^{θ}, 70^{θ} and 75.7^{θ} in the XRD pattern can be seen coming from the anatase TiO_2 lattice's crystal planes (1 0 1), (2 1 1), (0 0 4), (2 0 0), (1 0 5), (2 0 4), (2 2 0) and (2 1 5) respectively. This was matched to the anatase TiO_2 JCPDS file number 21-1272. According to Ba-abbad *et al*., the sharp peak at $2^{\theta} = 25.3$ validates the

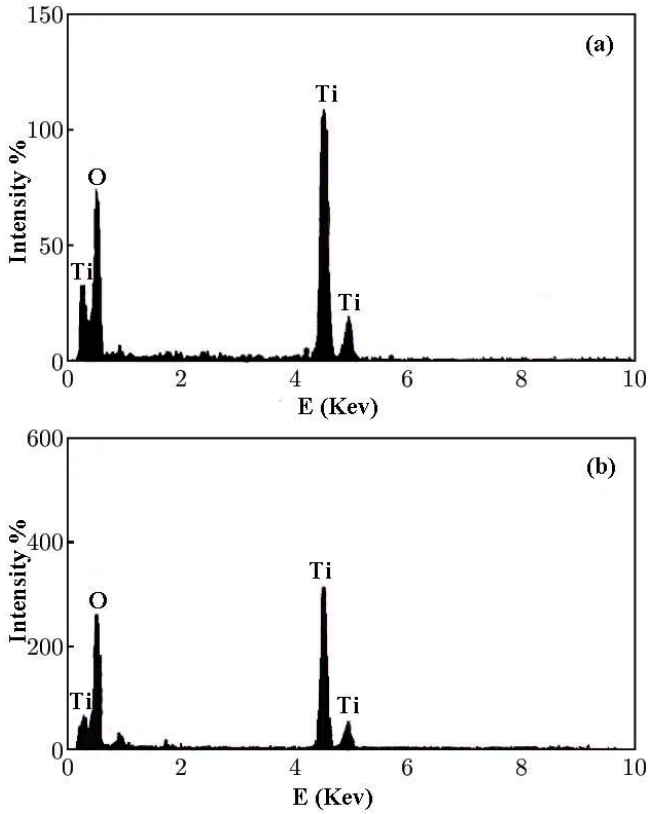

Fig. 8. Shows the EDX spectra of synthesized TiO_2-NPs samples using the hydrothermal method. (a): treated TiO_2-NPs; (b) untreated TiO_2-NPs.

Table 2. Shows the Dimensions of TiO_2 Nanoparticles with and without the Magnetic Field Affected by FE-SEM Image

Samples	D (nm)
Untreated TiO_2-NPs	72.55
Treated TiO_2-NPs	14.46

structure of the TiO_2 anatase. The brookite phase of TiO_2 is shown by the peak at 30.5 [28]. Figure 9b displays the untreated TiO_2-NPs lattice's XRD peaks from the (211) plane of TiO_2. For samples that had been treated with magnetic field, it was found that the peak intensity of new peak appeared in 28.3^{θ} and FWHM was increased. This shows that the treated TiO_2-NPs samples are well-crystalline as shown in Fig. 9a and Table 3.

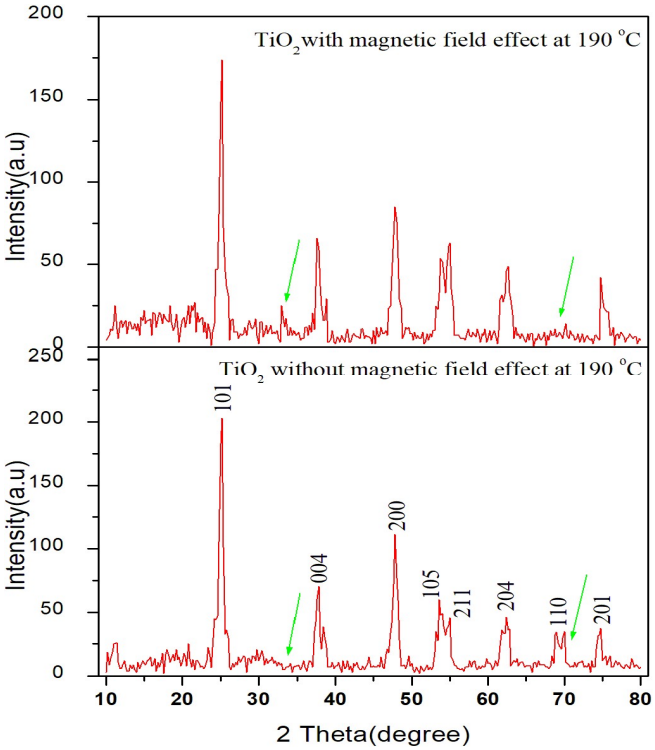

Fig. 9. XRD crystallography of synthesized TiO_2 nanoparticles by hydrothermal method (a) with magnetic field effect of 190 °C, and (b) without magnetic field effect at the same temperature.

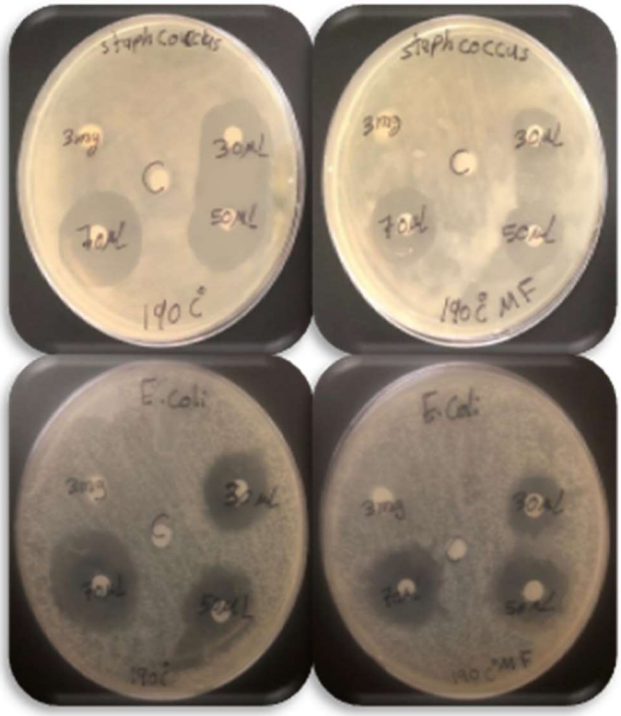

Fig. 10. Images of agar plate containing control as standard antibiotics and different concentrations of TiO_2 nanoparticles *i.e.*, 3 mg ml^{-1}, 30 µl ml^{-1}, 50 µl ml^{-1}, and 70 µl ml^{-1} of with and without influence magnetic field effect. Where, a for E. coli and b for Sauers.

Table 3. The Change in Crystal Sizes of Treated and Untreated TiO2-NPs Samples *via* (Calculated *via* Scherrer Equation)

Samples	D (nm)
Untreated TiO_2-NPs	12.55
Treated TiO_2-NPs	14.46

Antibacterial Activities Using Treated and Untreated TiO_2-NPs Samples

In the current study, the agar well diffusion technique was used to examine the antibacterial activity of synthetically produced untreated TiO_2-NPs and treated TiO_2-NPs against gram-negative (G-) and gram-positive (G+) bacterial strains. Both treated and untreated TiO_2-NPs nanoparticles at a concentration of 2.0 mg ml^{-1} were used for the antibacterial activity. Figure 10 displays the zone of inhibition for the treated and untreated TiO_2-NPs samples against *Escherichia coli* (*E. coli*-Gram-negative) and *Staphylococcus aureus* (*S. aureus*-Gram positive). Maximum activity was demonstrated against *E. coli* by untreated TiO_2-NPs. Similar findings were produced by Razi ahamed *et al.,* who reported that the antibacterial activity of TiO_2 nanoparticles synthesized by the Sol-gel method against *E. coli* using the disc diffusion method and the zones of inhibition were measured to be 17 mm for 100 g ml^{-1} concentration of TiO_2 nanoparticles [30]. According to Shokoh Parham *et al.,* investigation into the antibacterial properties of various metal oxide nanoparticles, the TiO_2 nanoparticles' photocatalytic properties are what give them their resistance to bacterial strains [31]. Against both gram-positive and gram-negative bacteria, Shagufta Naz *et al.,* demonstrated the antibacterial properties [32]. For treated TiO_2-NPs against *S. aureus*, the greatest zone was noted. Table 4 illustrates all the results of the antibacterial activities of both treated and untreated

Table 2. Shows the Test Results of Antibacterial Activity and Activity of Bacterial of TiO_2 Synthesized with and without Influence of Magnetic Field at Different Concertation

Human pathogenic bacteria	TiO_2 nanoparticles									
	Treated TiO_2-NPs.					Untreated TiO_2-NPs				
Zone of inhibition (mm)	3 mg ml^{-1}	30 µl	50 µl	70 µl	Control	3 mg ml^{-1}	30 µl	50 µl	70 µl	Control
S. aureus	2.9	6.2	8	10.4	0	1.2	8.1	11	12.2	0
E. coli	0.5	7.1	9.2	11	0	2.3	9	11.6	13	0

TiO_2-NPs. The obtained results are in high agreement with previously reported studies [33-36].

CONCLUSIONS

Hydrothermal technique has been used to synthesize titanium dioxide nanoparticles. Magnetic field treatment was applied during the synthesis of TiO_2 nanoparticles. The produced nanoparticles were crystallized, according to XRD Spectra. The maximum absorbance of the samples was shown by a red shift in the UV-Vis spectra of treated TiO_2 nanoparticles. The largest zone of inhibition against *E. coli* and the lowest zone of inhibition against *S. aureus* were seen in the untreated TiO_2 samples. When compared to the untreated TiO_2 samples, the treated samples showed increased antibacterial activity. The treated TiO_2-NPs exhibit a considerable improvement in antibacterial activity compared to the untreated TiO_2 nanoparticles and demonstrate the minimal viability percent for samples at a concentration of 30 mg ml^{-1}. Also, the photocatalytic properties of TiO_2-NPs have been evaluated using the photodegradation MB dye method and the results proved that the higher degrading percentage of MB dye (96%) has been seen during the use of treated TiO_2-NPs compared to untreated TiO_2-NPs which recorded 21%.

REFERENCES

[1] Sadiq, I. M.; Chowdhury, B.; Chandrasekaran, N.; Mukherjee, A., Antimicrobial sensitivity of Escherichia coli to alumina nanoparticles, *NBM.* **2009**, *5*, 282-286, DOI: 10.1016/j.nano.2009.01.002.

[2] Fu, G.; Vary, P. S.; Lin, C. -T., Anatase TiO_2 nanocomposites for antimicrobial coatings, *J. Phys. Chem. B,* **2005**, *109*, 8889-8898, DOI: 10.1021/jp0502196.

[3] Makhluf, S.; Dror, R.; Nitzan, Y.; Abramovich, Y.; Jelinek, R.; Gedanken, A., Microwave-assisted synthesis of nanocrystalline MgO and its use as a bacteriocide, *Adv. Funct. Mater.,* **2005**, *15*, 1708-1715, DOI: 10.1002/adfm.200500029.

[4] Rai, M.; Yadav, A.; Gade, A., Silver nanoparticles as a new generation of antimicrobials, *Biotechnol. Adv.,* **2009**, *27*, 76-83, DOI: 10.1016/j.biotechadv.2008.09.002.

[5] Shi, L. E.; Fang, X. J.; Zhang, Z. L.; Zhou, T.; Jiang, D.; Wu, H. H.; Tang, Z. X., Preparation of nano-ZnO using sonication method and its antibacterial characteristics, *Int. J. Food Sci.,* **2012**, *47*, 1866-1871, DOI: 10.1111/j.1365-2621.2012.03043.x.

[6] Xia, Y.; Yang, P.; Sun, Y.; Wu, Y.; Mayers, B.; Gates, B.; Yin, Y.; Kim, F.; Yan, H., One-dimensional nanostructures: synthesis, characterization, and applications, *Adv. Mater.,* **2003**, *15*, 353-389, DOI: 10.1002/adma.200390087.

[7] Jang, J. -M.; Kim, C. -R.; Ryu, H.; Razeghi, M.; Jung, W. G., ZnO 3D flower-like nanostructure synthesized on GaN epitaxial layer by simple route hydrothermal process, *J. Alloys Compd.,* **2008**, *463*, 503-510, DOI: 10.1016/j.jallcom.2007.09.077.

[8] Luo, Y.; Li, D.; Meng, Q., Towards Optimization of Materials for Dye-Sensitized Solar Cells, *Adv. Mater.,* **2009**, *21*, 4647-4651, DOI.10.1002/adma.200901078.

[9] Hu, C.; Lan, Y.; Qu, J.; Hu, X.; Wang, A., Ag/AgBr/TiO_2 visible light photocatalyst for destruction of azodyes and bacteria, *J. Phys. Chem. B.,* **2006**, *110*, 4066-4072,

DOI: 10.1021/jp0564400.

[10] Nosaka, Y.; Nosaka, A. Y., Generation and detection of reactive oxygen species in photocatalysis, *Chem. Rev.,* **2017**, *117*, 11302-11336, DOI: 10.1021/acs.chemrev.7b00161.

[11] Huang, H.; Xiao, K.; He, Y.; Zhang, T.; Dong, F.; Du, X.; Zhang, Y., *In situ* assembly of BiOI@$Bi_{12}O_{17}Cl_2$ pn junction: charge induced unique front-lateral surfaces coupling heterostructure with high exposure of BiOI {001} active facets for robust and nonselective photocatalysis, *Appl. Catal.,* **2016**, *199*, 75-86, DOI: 10.1016/j.apcatb.2016.06.020.

[12] Etacheri, V.; Michlits, G.; Seery, M. K.; Hinder, S. J.; Pillai, S. C., A highly efficient TiO_2-xCx nano-heterojunction photocatalyst for visible light induced antibacterial applications, *ACS Appl. Mater. Interfaces.,* **2013**, *5*, 1663-1672, DOI: 10.1021/am302676a.

[13] Battin, T. J.; Kammer, F. V. D.; Weilhartner, A.; Ottofuelling, S.; Hofmann, T., Nanostructured TiO_2: transport behavior and effects on aquatic microbial communities under environmental conditions, *Environ. Sci. Technol.,* **2009**, *43*, 8098-8104, DOI: 10.1021/es9017046.

[14] Kitahama, Y.; Sakaguchi, Y., Magnetic isotope effect on kinetic parameters and quantum beats of radical pairs in micellar solution studied by optically detected ESR using pulsed microwave, *J. Phys. Chem. A.,* **2008**, *112*, 176-182, DOI: 10.1021/jp076611w.

[15] Miura, T.; Murai, H., Real-time observation of the spin-state mixing process of a micellized radical pair in weak magnetic fields by nanosecond fast field switching, *J. Phys. Chem. A.,* **2008**, *112*, 2526-2532, DOI: 10.1021/jp077505x.

[16] Henbest, K. B.; Kukura, P.; Rodgers, C. T.; Hore, P. J.; Timmel, C. R., Radio frequency magnetic field effects on a radical recombination reaction: a diagnostic test for the radical pair mechanism, *J. Am. Chem. Soc.,* **2004**, *126*, 8102-8103, DOI: 10.1021/ja048220q.

[17] Yamaguchi, M.; Tanimoto, Y.; Yamaguchi, M., *Magneto-science: magnetic field effects on materials: fundamentals and applications*, *Springer*, **2006**, 112, DOI: 10.1007/978-3-540-37062-8.

[18] Aravind, M.; Amalanathan, M.; Mary, M., Synthesis of TiO_2 nanoparticles by chemical and green synthesis methods and their multifaceted properties, *SN Appl. Sci.,* **2021**, *3*, 1-10, DOI: 10.1007/s42452-021-04281-5.

[19] Thinkohkaew, K.; Piroonpan, T.; Jiraborvornpongsa, N.; Potiyaraj, P., Development of multifunctional polypropylene nonwoven fabric by radiation induced grafting of TiO_2 nanoparticles and trifluoroethyl methacrylate for protective textile applications, *Materialia.* **2022**, *21*, 101355, DOI: 10.1016/j.mtla.2022.101355.

[20] Bermudez, P. R.; Rodríguez, V. A.; Peña-Rodríguez, G., Electrochemical synthesis of titanium dioxide nanostructures and its application in the in dye photocatalytic removal, *J. Phys. Conf. Ser.,* **2021**, *2046*, 012041, DOI: 10.1088/1742-6596/2046/1/012041/meta.

[21] Ko, S.; Banerjee, C. K.; Sankar, J., Photochemical synthesis and photocatalytic activity in simulated solar light of nanosized Ag doped TiO_2 nanoparticle composite, *Compos. B. Eng.,* **2011**, *42*, 579-583, DOI: 10.1016/j.compositesb.2010.09.007.

[22] Darr, J. A.; Zhang, J.; Makwana, N. M.; Weng, X., Continuous hydrothermal synthesis of inorganic nanoparticles: applications and future directions, *Chem. Rev.,* **2017**, *117*, 11125-11238, DOI: 10.1021/acs.chemrev.6b00417.

[23] Nadimpalli, N. K. V.; Bandyopadhyaya, R.; Runkana, V., Thermodynamic analysis of hydrothermal synthesis of nanoparticles, *Fluid Phase Equilibria.* **2018**, *456*, 33-45, DOI: 10.1016/j.fluid.2017.10.002.

[24] Pukkella, A. K.; Nadimpalli, N. R. V.; Runkana, V.; Subramanian, S., A novel spiral infinity reactor for continuous hydrothermal synthesis of nanoparticles, *Sci. Rep.,* **2022**, *12*, 1-16, DOI: 10.1038/s41598-022-11141-8.

[25] Trinh, T. T. P. N. X.; Giang, N. T. H.; Thinh, D. B.; Dat, N. M.; Trinh, D. N.; Hai, N. D.; Oanh, D. T. Y.; Nam, H. M.; Phong, M. T.; Hieu, N. H., Hydrothermal synthesis of titanium dioxide/graphene aerogel for photodegradation of methylene blue in aqueous solution, *J. SCI.-ADV. MATER. DEV.,* **2022**, *7*, 100433, DOI: 10.1016/j.jsamd.2022.100433.

[26] Gan, Y. X.; Jayatissa, A. H.; Yu, Z.; Chen, X.; Li, M. Hydrothermal synthesis of nanomaterials, *J. Nanomater*., **2020**, *2020*, 1-3,

DOI: 10.1155/ 2020/8917013.

[27] Vilas, V.; Philip, D.; Mathew, J., Biosynthesis of Au and Au/Ag alloy nanoparticles using Coleus aromaticus essential oil and evaluation of their catalytic, antibacterial and antiradical activities, *J. Mol. Liq.,* **2016**, *221*, 179-189, DOI: 10.1016/ j.molliq.2016.05.066.

[28] Ba-Abbad, M. M.; Kadhum, A. A. H.; Mohamad, A. B.; Takriff, M. S.; Sopian, K., Synthesis and catalytic activity of TiO_2 nanoparticles for photochemical oxidation of concentrated chlorophenols under direct solar radiation, *Int. J. Electrochem. Sci.* **2012**, *7*, 4871-4888.

[29] Hasan, N.; Wu, H. F.; Li, Y. -H.; Nawaz, M., Two-step on-particle ionization/enrichment *via* a washing-and separation-free approach: multifunctional TiO_2 nanoparticles as desalting, accelerating, and affinity probes for microwave-assisted tryptic digestion of phosphoproteins in ESI-MS and MALDI-MS: comparison with microscale TiO_2, *Anal. Bioanal. Chem.,* **2010**, *396*, 2909-2919, DOI: 10.1007/s00216-010-3573-3.

[30] Elahi, S. M.; Dalouji, V.; Mehrparvar, D.; Valedbagi, S., Influence of deposition rate on optical properties of RF-magnetron sputtered carbon-nickel composite films deposited at different deposition times, *Mol. Cryst. Liq.,* **2013**, *587*, 105-112, DOI: 10.1080/ 15421406.2013.821586.

[31] Parham, S.; Wicaksono, D. H. B.; Bagherbaigi, S.; Lee, S. L.; Nur, H., Antimicrobial treatment of different metal oxide nanoparticles: a critical review, *J. Chin. Chem. Soc.,* **2016**, *63*, 385-393, DOI: 10.1002/ jccs.201500446.

[32] Singh, J.; Mohapatra, S., Thermal evolution of structural, optical and photocatalytic properties of TiO_2 nanostructures, *Adv. Mater. Lett.,* **2015**, *6*, 924-929, DOI: 10.5185/amlett.2015.6000.

[33] Abdulrahman, A.; Mohammed, H., Temperature and Solvent Impact on Zinc Oxide Nanostructures Synthesized *via* Hydro-Solvo-Thermal Technique, IJSR., **2017**, *6.11*, 1132-1136. DOI: org/10.21275/ART20177913.

[34] Abdulredha, S. T.; Abdulrahman, N. A., Cu-ZnO Nanostructures Synthesis and Characterization. *Iraqi J.* Sci., **2021**, *4*, 708-717. DOI: org/10.24996/ijs.2021.62.3.1

[35] Al-Hakeem, M. H.; Abdulrahman; N. A., Alsammaraie, A. A., Preparation and characterization of Co doped ZnO nanoparticles., *Solid State Technology*, **2020**, *7*, 636-644.

[36] Abdulsada, R. O.; Thamir, A. A. H., Synthesis of TiO_2 Thin Films Nanoparticles with Different Layers using Simple Sol-Gel Method., *Iraqi J. Sci.,* **2021**, *5*, 4425-4429. DOI: org/10.24996/ijs.2021.62.11(SI).23.